Supporting Information

Multifunctional High-activity and Robust Electrocatalyst Derived from Metal-organic Frameworks

Erhuan Zhang,[1,2] Yu Xie,[1*] Suqin Ci,[1] Jingchun Jia,[2,3] Pingwei Cai,[1,2] Luocai Yi,[1] Zhenhai Wen[1,2,3*]

1 Key Laboratory of Jiangxi Province for Persistent Pollutants Control and Resources Recycle, Nanchang Hangkong University, Nanchang 330063, P. R. China

2 Key Laboratory of Design and Assembly of Functional Nanostructures, Fujian Institute of Research on the Structure of Matter, Chinese Academy of Sciences, Fuzhou, Fujian 350002, P. R. China

3 Fujian Provincial Key Laboratory of Nanomaterials, Fujian Institute of Research on the Structure of Matter, Chinese Academy of Sciences, Fuzhou, Fujian 350002, P. R. China

E-mail: *xieyu_121@163.com, wen@fjirsm.ac.cn*

Table of Contents:

Part I: Experimental section

1.1. Electrochemical measurements

HER tests:

The working electrode was prepared by following the steps below: (i) Glassy carbon electrode (GCE, φ: 3.0 mm) were firstly polished using aluminum oxide (Al_2O_3, 0.05 μm) powder followed by rinsing thoroughly with deionized water and dried at room temperature; (ii) 2.5mg electrode materials were dispersed in a mixture of 0.05 mL Nafion (5%), 0.05mL ethanol and 0.45 mL distilled water; (iii) The suspension was obtained under ultrasonic agitation for 30 minutes; (iiii) Then 6 μL of the solution was drop-casted onto the GCE to achieve a catalyst loading of ~0.425 mg cm^{-2} and dried under room temperature. The electrocatalytic properties of the compounds for hydrogen evolution reaction (HER) was measured by a three-electrode system on Instruments760D electrochemical workstation at room temperature. The active film deposited on glassy carbon (GC) electrode, a Pt wire as the counter electrode, and an Ag/AgCl electrode as the reference electrode were applied to fabricate a three-electrode electrochemical cell. All potentials, measured against Ag/AgCl reference electrode, were calibrated to reversible hydrogen electrode (RHE) scale using the following Equation: E (RHE) = E (Ag/AgCl) + 0.197 V+ 0.059×pH. Electrochemical measurements of active materials for Linear sweep voltammograms (LSV) and i-t curves were measured in 0.5 M H_2SO_4 (pH = 0), 0.1 M phosphate buffer (pH = 7) and 0.1 M KOH (pH = 13); these act as electrolytes. Before and during experiments, the electrolytes were saturated with Ar. For all of the experiments mentioned above, the electrodes were cycled at a scan rate of 50 mV s^{-1} until reproducible CVs were obtained.

ORR tests:

Electrocatalytic activities for ORR of the as-prepared catalysts were evaluated by CV, rotating disk electrode (RDE) and rotating ring-disk electrode (RRDE) with a three-electrode cell system on a CHI-760 electrochemical workstation (CH Instruments). Working electrode was prepared as described above in HER, transferred to 0.1 M KOH. 0.5 M H_2SO_4 or 0.1 M sodium phosphate electrolyte at room temperature. CV measurements using three-electrode cell were performed in the above-mentioned

electrolyte with polished Pt wires as counter electrode, and Ag/AgCl (saturated KCl) as the reference electrode. Prior to measurements, Ar or O_2 was used to purge the solution to achieve an O_2-free or O_2-saturated condition. The samples were repeatedly swept between -0.8↔+0.2 V (base). 0↔+1.0 V (acid) or -0.4↔+0.6 V (neutral) (vs Ag/AgCl) with a scan rate of 50 mV s^{-1} at 25 °C till a steady voltammogram curve had been obtained. In comparison, commercial 20 wt % platinum on carbon black (Pt/C) was also measured under the identical condition. RDE measurements were scanned at a rate of 5 mV s^{-1} with different rotating speeds from 400 to 2500 rpm. Koutecky-Levich plots were analyzed at various electrode potentials. All potentials were calibrated to reversible hydrogen electrode (RHE) scale.

To further investigate ORR activity at a RDE, the slopes of their best linear fit lines were used to calculate the number of electrons transformed in oxygen reduction according to K-L equations (1) and (2):

$$\frac{1}{j}=\frac{1}{j_L}+\frac{1}{j_K}=\frac{1}{B\omega^{1/2}} \quad (1)$$

$$B = 0.62nFC_0(D_0)^{2/3}V^{-1/6} \quad (2)$$

Where j_L is the measured current; j_K is the kinetic-limiting current and w is the electrode rotation rate; n is the overall number of transferred electrons in the ORR process; F is the Faradaic constant (96485 C/mol), C_O is the oxygen concentration (solubility) in 0.1 M KOH (1.2×10^{-6} mol cm^{-3}); D_O is the oxygen diffusion coefficient in 0.1 M KOH (1.90×10^{-5} cm^2 s^{-1}) and v is the kinematic viscosity of the 0.1 M KOH (0.01 cm^2 s^{-1}).

For the RRDE measurements, catalyst inks and electrodes were prepared by the same method as for RDE. The disk electrode was scanned at a rate of 5 mV s^{-1}, and the ring potential was constant at 1.5 V vs RHE. The H_2O_2 yield and transfer number (n) were determined by the followed equations:

$$\%(H_2O_2) = 200\frac{I_r/N}{I_d + I_r/N} \quad (3)$$

$$n = 4\frac{I_d}{I_d + I_r/N} \quad (4)$$

Where Id is the disk current, and Ir is the ring current, and N is current collection efficiency of the Pt ring. N is 0.44 from the reduction of $K_3Fe[CN]_6$.

GOR measurement:

Evaluation of the catalytic performance for glucose as follows: The electrochemical measurements were performed in a conventional three-electrode cell controlled at room temperature using CHI 760 workstation (CH Instruments) in 0.1 M KOH electrolyte, in which the glassy carbon modified with Co@NCNT was used as the working electrode, a platinum wire as counter electrode and Ag/AgCl electrode as reference electrode, respectively. To prepare the working electrode, prior to use, the glass carbon electrode (GCE) was polished with alumina slurry, and then ultrasonically cleaned alternately in ethanol and double-distilled water, 2.5 mg was dispersed in a mixture of 0.05 mL Nafion and 0.03mL ethanol, finally add distilled water to 0.5 mL volume solution. A suspension was obtained under ultrasonic agitation for more than 30 minutes. Typically, 6 μL of the well-ultrasounded mixture was dropped and adhered onto the cleaned and dried GCE and allowed to dry at room temperature. Meanwhile, all solutions were deoxygenated with highly pure argon (99.99%) for at least 15 min before tests. In this work, all potentials were referred to Ag/AgCl reference electrode, the geometric surface area of the modified electrode (0.07 cm^2) was used to calculate current density. The electrochemical glucose detection performance was investigated by CV in the region from 0.864 V to 1.564 V and chronoamperometry. All potentials were calibrated to reversible hydrogen electrode (RHE) scale.

OER tests:

The working electrode was prepared by the similar method in the HER measurement above. The electrocatalytic properties of the compounds for oxygen evolution reaction (OER) was measured by a three-electrode system on Instruments760D electrochemical workstation at room temperature. The active film deposited on glassy carbon (GC) electrode, a Pt wire as the counter electrode, and an Ag/AgCl electrode as the reference electrode were applied to fabricate a three-electrode electrochemical cell. All potentials, measured against Ag/AgCl reference electrode, were calibrated to reversible hydrogen electrode (RHE) scale using the following Equation: E (RHE) = E (Ag/AgCl) + 0.197 V+ 0.059×pH. Electrochemical measurements of active materials for Linear sweep

voltammograms (LSV) were measured in 1 M KOH (pH = 14) electrolyte. For all of the experiments mentioned above, the electrodes were cycled at a scan rate of 50 mV s^{-1} until reproducible CVs were obtained.

Zinc-air battery measurement:

For the zinc-air battery tests, the electrode was prepared by uniformly coating the as-prepared catalyst ink onto hydrophobic carbon paper electrode then drying it at 80 °C for 2 h. This catalyst ink was uniformly dropcasted onto 1 cm^{-2} of carbon paper to achieve a catalyst loading of 1 mg cm^{-2}. A Zn plate was used as the anode. Both electrodes were assembled into customized electrochemical cell, and 6 M KOH aqueous solution was used as the electrolyte.

Part II: Characterization of the samples

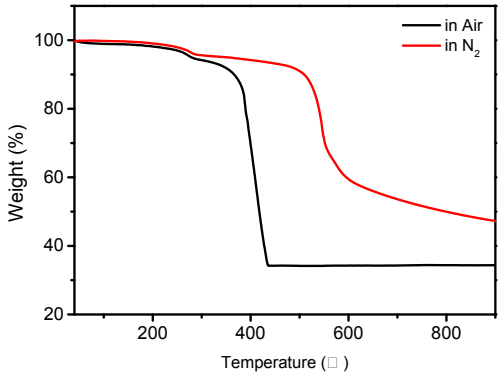

Fig. S1. Thermogravimetric analysis (TGA) curves of ZIF-67 with a ramp of 10 ºC min^{-1} at flowing N_2 and Air.

Thermogravimetric analyses (TGA) of ZIF-67 were performed under N_2 and air flowing at a heating ramp of 10 ºC, which represent the complete decomposition of ZIF-67 above 700 ºC (Figure S1).

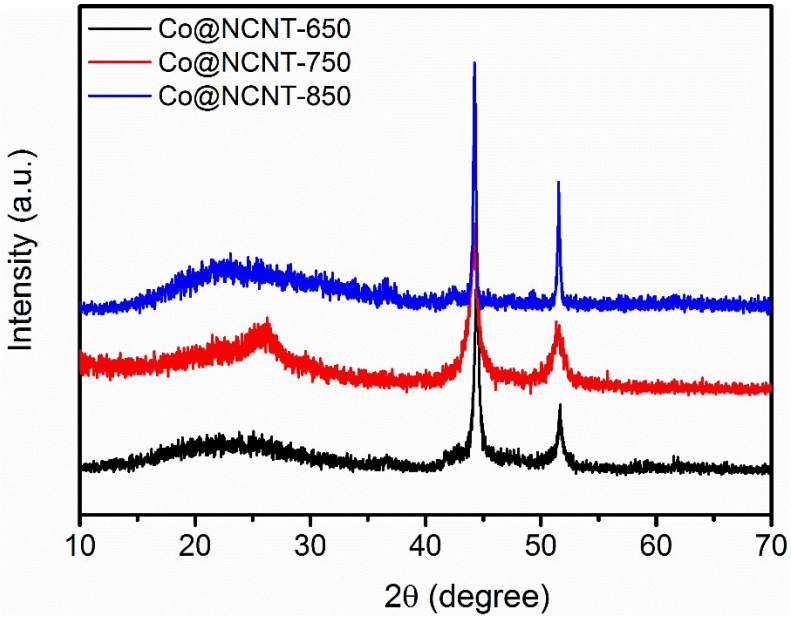

Fig. S2. XRD patterns of Co@NCNT-650, Co@NCNT-750, Co@NCNT-850. In addition, Co@NCNT-750 was denoted as Co@NCNT.

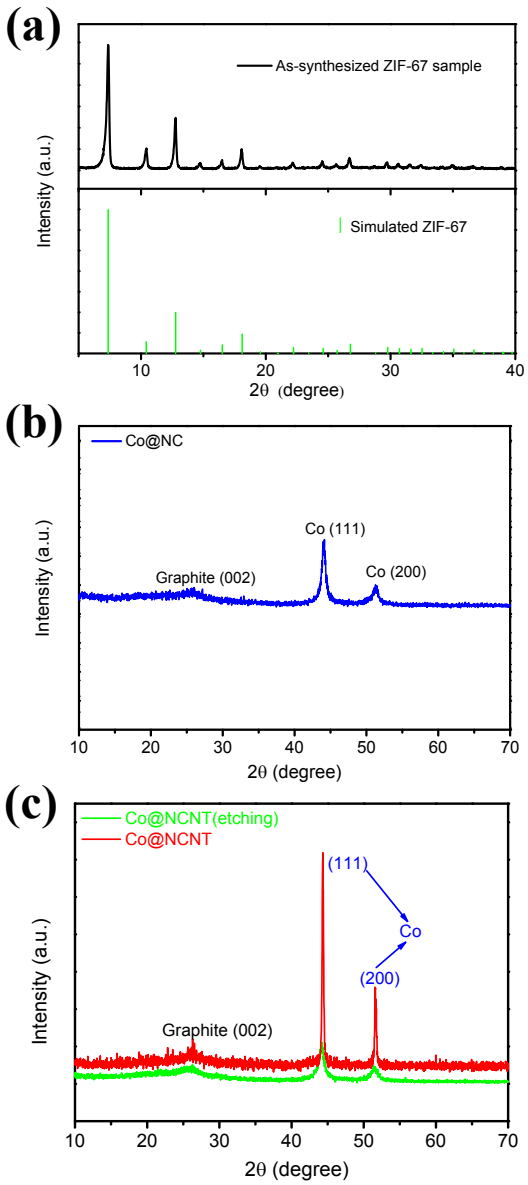

1

2 Fig. S3. XRD patterns of (a) ZIF-67 Precursor, (b) Co@NC, (c) Co@NCNT (red) and
3 Co@NCNT after etching for 24 h (green).

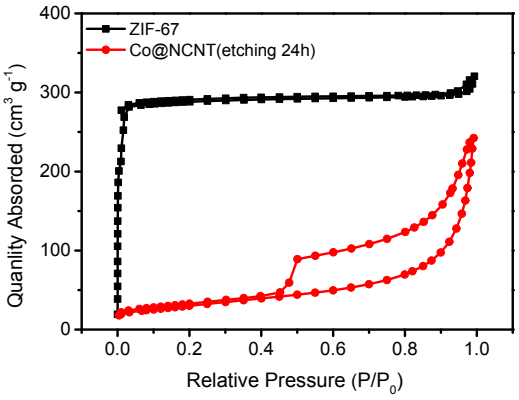

Figure S4. Nitrogen adsorption/desorption isotherms of ZIF-67 and Co@NCNT (etching).

According to the N_2 adsorption-desorption isotherms, The Brunauer-Emmett-Teller (BET) surface area for ZIF-67 and Co@NCNT (etching) were estimated to be 911.9 and 107.8 m^2 g^{-1}, respectively.

Part III: Electrochemical testing results

HER

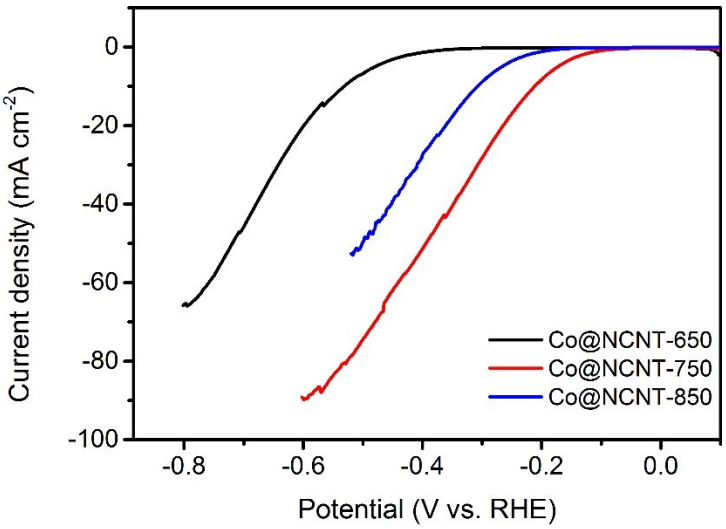

Fig. S5. (a) Linear sweep voltammetry (LSV) curves in 0.5 M H_2SO_4 (pH = 0). The mixture of ZIF-67 and proper amounts of dicyandiamide was annealed at 650, 750, and 850 ºC for 2 h (denoted as Co@NCNT-650, Co@NCNT-750 and Co@NCNT-850).

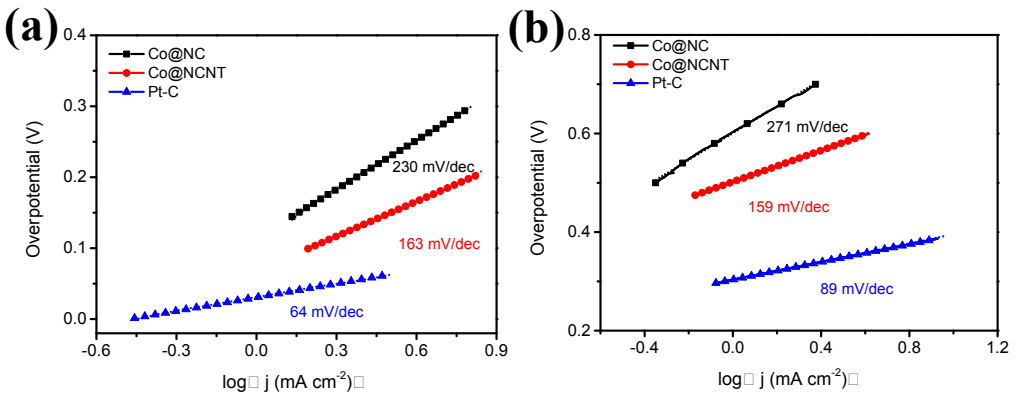

Fig. S6. Tafel plots in 0.1M KOH (a, pH =13) and 0.1 M buffer (b, pH = 7).

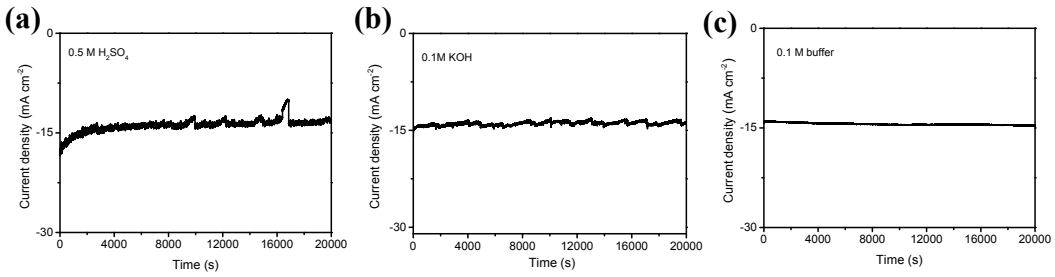

Fig. S7. HER stability tests of the Co@NCNT in 0.5 M H_2SO_4 (a), 0.1M KOH (b) and 0.1M buffer (c).

Time dependence of the current density for Co@NCNT at a static potential of -0.3 V in 0.1 M KOH and -0.8 V in 0.1 M buffer for 20000 s.

ORR Test

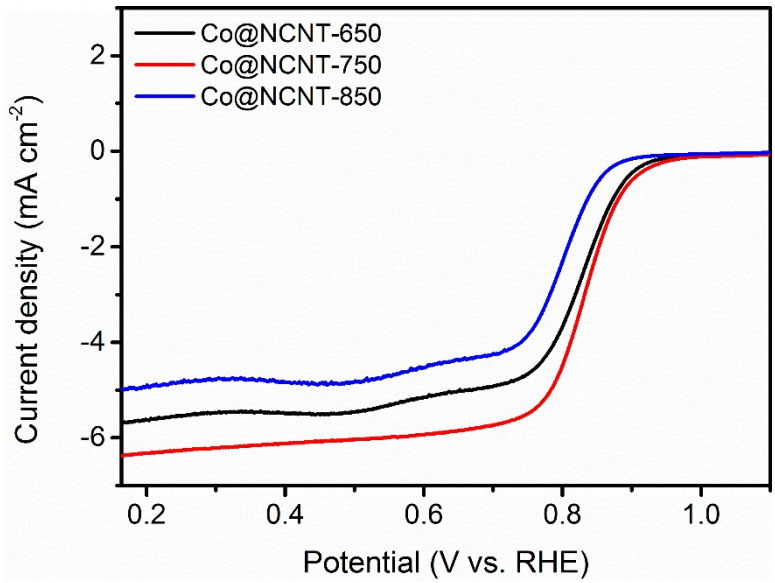

Fig. S8. LSV curves of Co@NCNT-650, Co@NCNT-750 and Co@NCNT-850 in oxygen-saturated 0.1 M KOH with rotation rate of 1600 rpm.

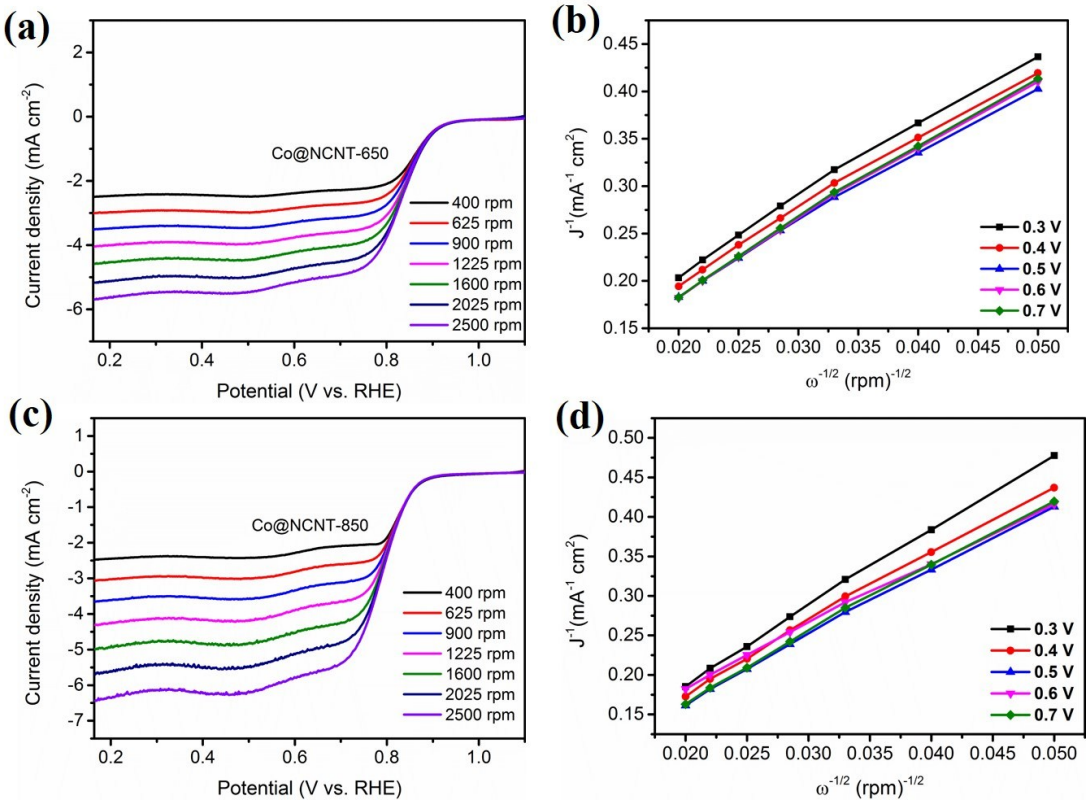

Fig. S9. (a), (c) ORR polarization curves of Co@NCNT-650, Co@NCNT-850 at different rotating speeds, (b), (d) K-L plots of Co@NCNT-650, Co@NCNT-850 at different potentials.

RDE measurements at various rotating speeds at a scan rate of 5 mV s^{-1} in an O_2-saturated system are carried out and the Koutecky-Levich (K-L) equation is used to analyze the kinetic parameters of Co@NCNT-650 and Co@NCNT-850.

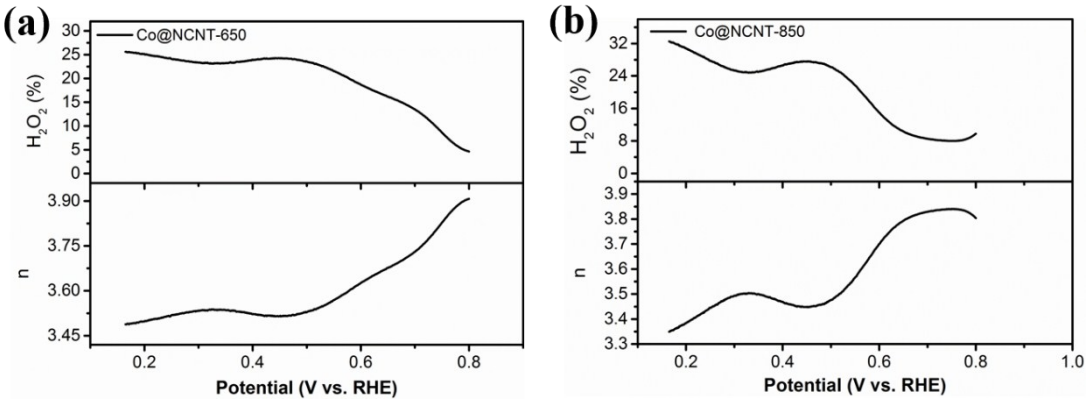

Fig. S10. (a), (b) Peroxide yields and electron transfer numbers (n) of Co@NCNT-650, Co@NCNT-650 at various potentials based on RRDE data.

To quantify the ORR pathway, a rotating ring-disk electrode (RRDE) technique is conducted to monitor the electron transfer numbers and formation of HO_2^{-1} during the ORR process. Fig. S10 reveals that the measured yields of HO_2^{-1} generated at the disk electrode vary over the potential range. The HO_2^{-1} yield for Co@NCNT-650 is below 25.6 % with n of 3.48-3.90. Whereas, the Peroxide yield for Co@NCNT-850 is below 32.5 % with n of 3.34-3.80.

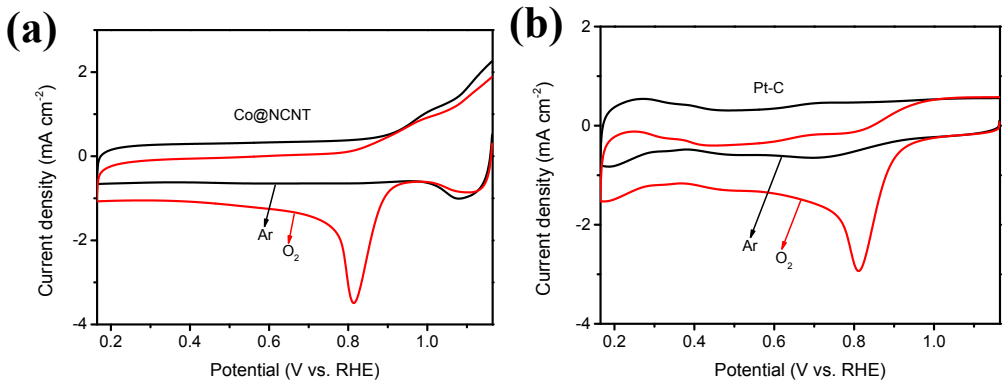

Fig. S11. CV curves of (a) Co@NCNT and (b) Pt/C in O_2 and Ar-saturated 0.1 M KOH solution.

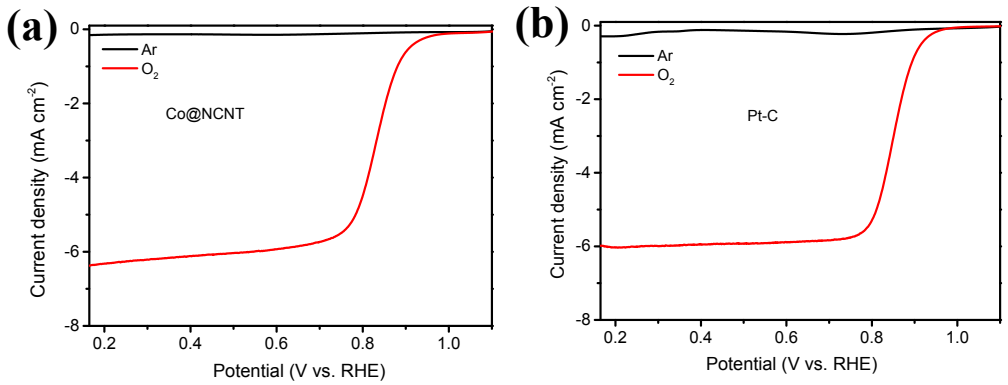

Fig. S12. LSV curves of (a) Co@NCNT and (b) Pt/C in O_2 and Ar-saturated 0.1 M KOH solution, respectively.

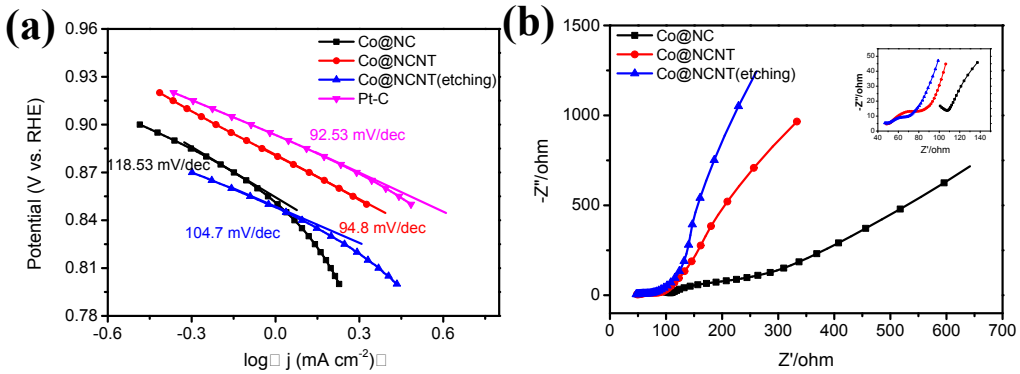

Fig. S13. (a) Tafel plots for Co@NC, Co@NCNT, Co@NCNT after etching and Pt-C derived from the corresponding RDE data in O_2-saturated 0.1 M KOH solution, (b) Nyquist plots of Co@NC, Co@NCNT and Co@NCNT (etching) at a bias of open potential in O_2-saturated 0.1 M KOH solution.

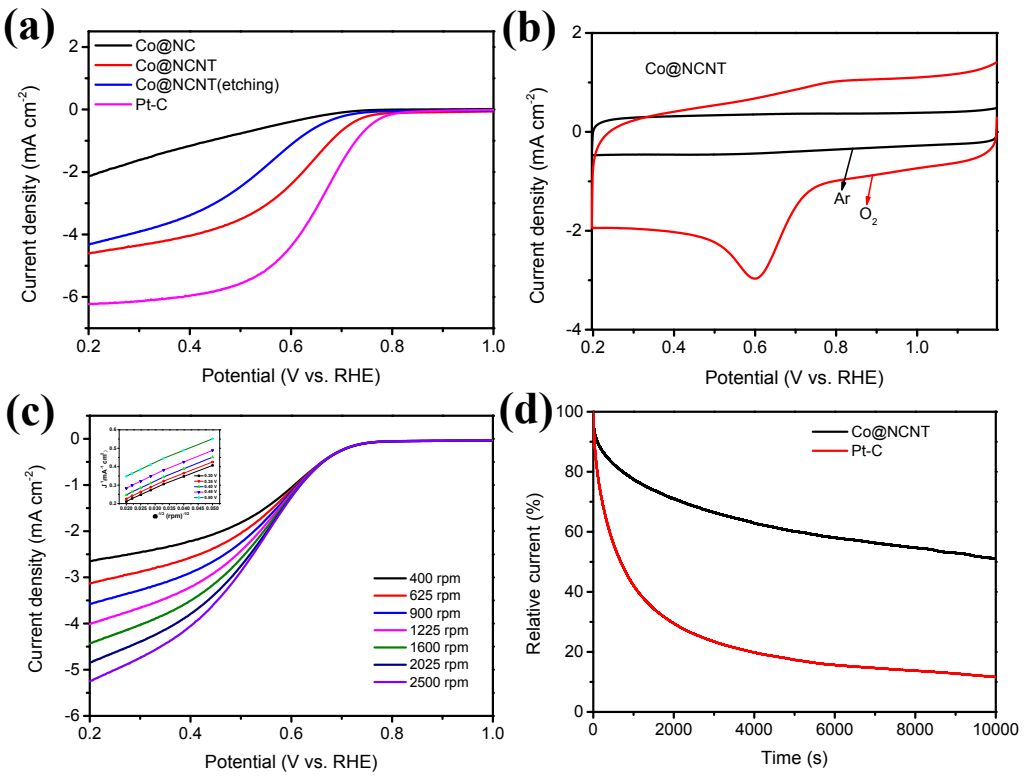

Fig. S14. (a) RDE polarization curves of Co@NC, Co@NCNT, Co@NCNT after etching and Pt-C in O_2-saturated 0.5 M H_2SO_4 with a sweep rate of 5 mV/s and rotation rate of 1600 rpm, (b) CV curves of Co@NCNT in O_2 and Ar-saturated 0.5 M H_2SO_4 solution, (c) LSV curves of Co@NCNT at various speeds (inset: K-L plots for Co@NCNT at various potentials), (d) Current-time chronoamperometric responses of Co@NCNT and commercial Pt/C at a constant voltage of 0.6 V in O_2-saturated 0.1 M KOH solution (1600 rpm).

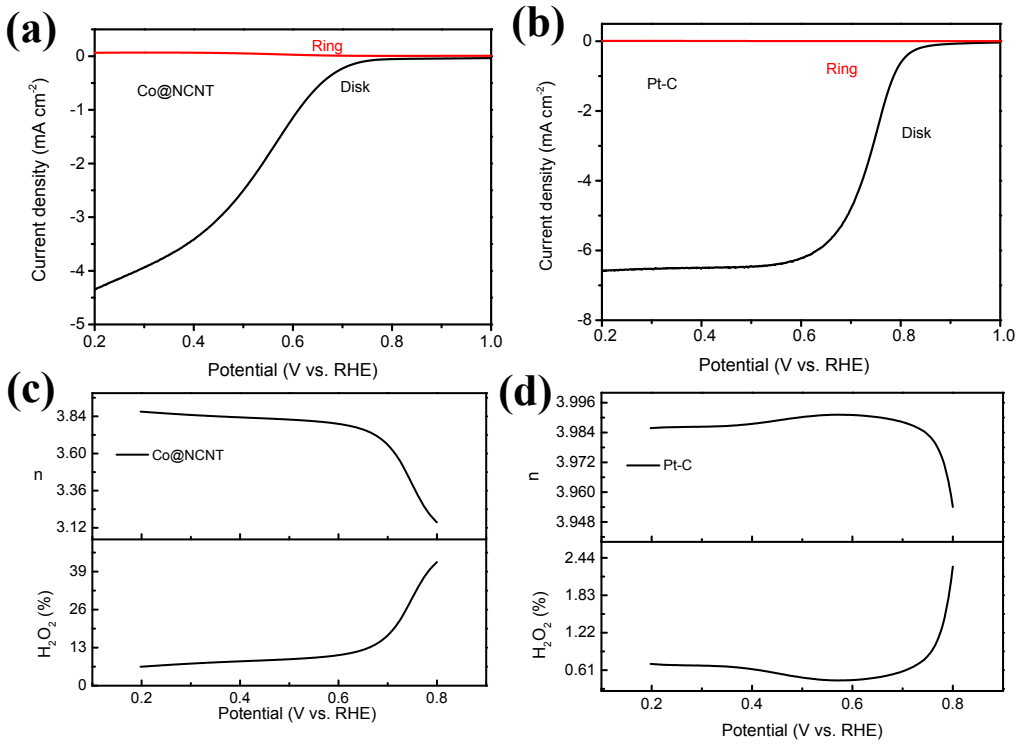

Fig. S15. Rotating ring-disk electrode voltammograms recorded with Co@NCNT (a) and commercial Pt/C (b) in O_2-saturated 0.5 M H_2SO_4 at 1600 rpm, the calculated electron transfer number and H_2O_2 during ORR catalyzed by Co@NCNT (c) and commercial Pt/C (d).

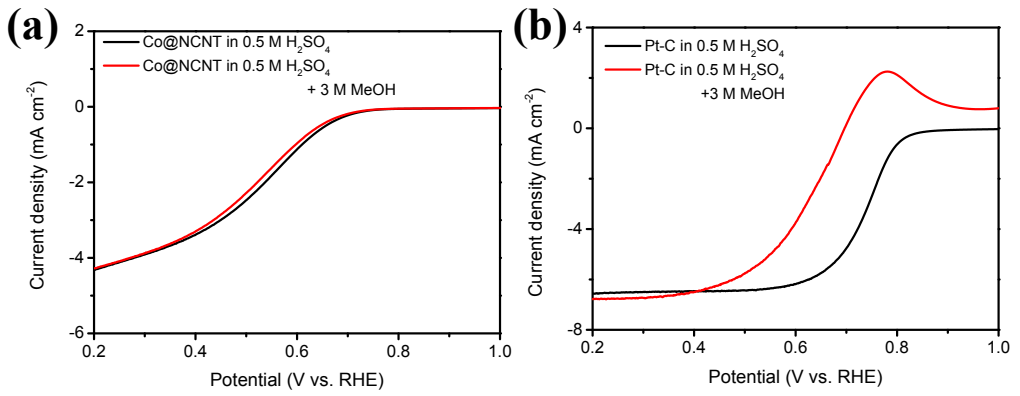

Fig. S16. Co@NCNT (a) and commercial Pt/C (b) in O_2-saturated 0.5 M H_2SO_4 without (black line) and with (red line) 3 M MeOH.

Glucose oxidation:

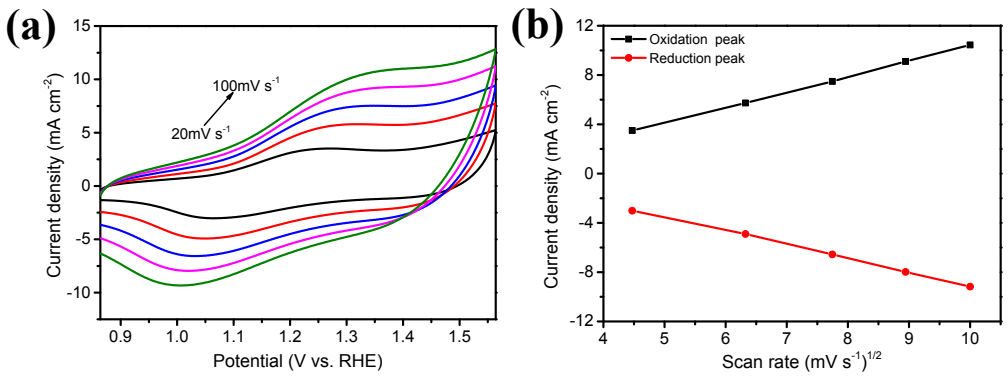

1

2 Fig. S17. (a) CVs of Co@NCNT/GCE at different scan rates from 20 mV s^{-1}-100 mV
3 s^{-1}, (b) plots of peak currents vs. the square root of the scan rate.

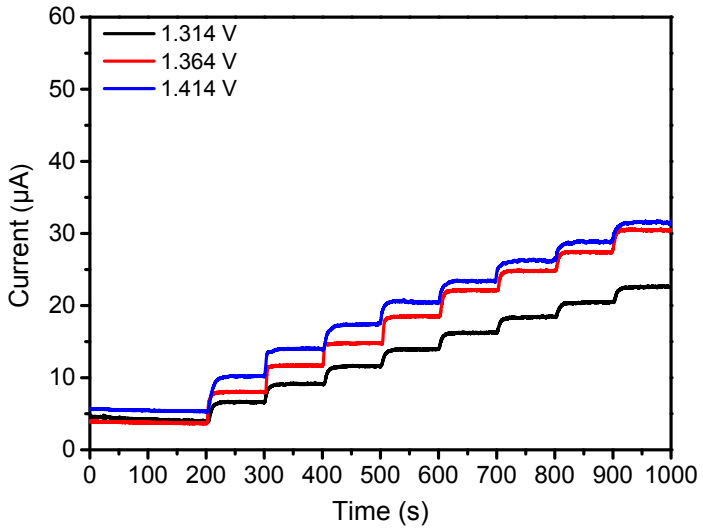

4

5 Fig. S18. Amperometric response of Co@NCNT/GCE at different potentials with
6 dropwise addition of 0.2 mM glucose into 0.1 M KOH solution at 100 s interval (applied
7 potential: 1.314 V-1.414V).

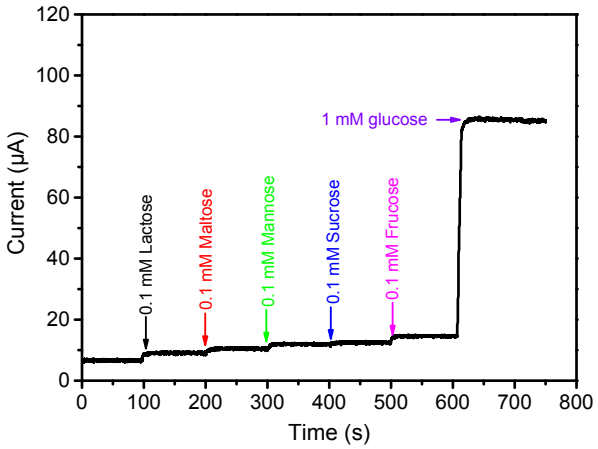

Fig. S19. Amperometric response of Co@NCNT/GCE to the continuous addition of 0.1 mM Lactose, 0.1 mM Maltose, 0.1 mM Mannose, 0.1 mM Sucrose, 0.1 mM Fructose, and 1mM glucose at a potential of 1.364 V.

Table S1. Chemical composition of the samples

Sample	N (wt %)[1]	C (wt %)[1]	H (wt %)[1]	Co(wt %)[2]
Co@NC	2.38/2.60	44.92/34.94	1.18/1.14	45.81%
Co@NCNT	3.08/3.18	53.00/43.12	0.53/0.50	39.53%
Co@NCNT(etching）	2.02/2.01	75.77/75.98	0.90/0.88	12.46%

Note: [1]Measured by elemental analysis; [2]Measured by inductively Coupled Plasma-Optical Emission Spectroscopy Measurement.

Table S2. HER performance for Co@NCNT under different conditions.

Catalyst	b (mV dec^{-1})[1]	J (mA cm^{-2})[2]	η_{10} (mV)[3]	J_0 (mA cm^{-2})[4]	Different solutions
Co@NCNT	93	10	210	0.078	Acidic solution
Co@NCNT	163	10	244	0.39	Basic solution
Co@NCNT	159	10	670	4.79×10^{-3}	Neutral solution

Note: [1] represents Tafel slope (mVdec^{-1}), [2] represents current density (mA cm^{-2}), [3] represents corresponding overpotential (η) at the current density of 10 mA cm^{-2}, [4] represents exchange current density (mA cm^{-2}).

Table S3. Comparison of the ORR performance for Co@NCNT with some representative catalysts recently reported in 0.1 M KOH solution.

Catalyst	Half-wave potential	Diffusion limited current	Electron-transfer number	Tafel slope	H_2O_2 yield	Reference
Co@NCNT	0.828	-6.3 mA cm^{-2}	3.95-3.99	94.8 mV/decade	＜4.5%	This work
P-CNCo-20	0.84	-5.1 mA cm^{-2}	3.9	N/A	N/A	[1]
Co-N-C	0.871	-5.35 mA cm^{-2}	3.84-4.00	N/A	＜7.0%	[2]
CNT/Fe_3C	N/A	N/A	3.99	91.2 mV/decade	＜7.7%	[3]
Fe_3C/C-800	0.83	N/A	3.8-4.0	N/A	18%	[4]
N-Co_9S_8/G	N/A	N/A	3.7-3.9	N/A	＜5%	[5]
Co@Co_3O_4@C-CM	0.81 V	N/A	3.8-3.9	N/A	N/A	[6]
Co/NG	N/A	-8.0 mA cm^{-2}	3.8	N/A	N/A	[7]
N/Co-doped PCP// NRGO	0.86	-7.53 mA cm^{-2}	3.90-3.94	85 mV/decade	N/A	[8]
LDH@ZIF-67-800	0.83	-5.5 mA cm^{-2}	3.86-3.98	63-115 mV/decade	＜10%	[9]
Co-C@Co_9S_8 DSNCs	N/A	N/A	3.8	N/A	N/A	[10]
NCNTFs	0.87 V	N/A	3.96-4.00	~64 mV/decade	＜1.6%	[11]
Carbon-L	0.70 V	-4.6 mA cm^{-2}	3.68	N/A	N/A	[12]
Z8-Te-1000	0.80	N/A	~4.0	N/A	N/A	[13]
GNPCSs-800	N/A	-6 mA cm^{-2}	3.78-3.98	N/A	＜10%	[14]
Co,N-CNF	0.81	-5.71 mA cm^{-2}	3.8	60 mV mV/decade	N/A	[15]

Table S4. Comparison of the ORR performance for Co@CNT with some representative catalysts recently reported in acid (0.5 M H_2SO_4 or 0.1 M $HClO_4$) solutions.

Catalyst	Half-wave potential	Diffusion limited current	Electron-transfer number	Tafel slope	H_2O_2 yield	Reference
Co@NCNT	0.605 V	-4.61mA cm^{-2}	3.16-3.86	N/A	< 42%	This work
P-CNCo-20	0.761	-5.1 mA cm^{-2}	3.9	N/A	N/A	[1]
Co-N-C	0.761	-6.02 mA cm^{-2}	＞3.94	93 mV/decade	< 3.1%	[5]
CNT/Fe_3C	N/A	N/A	N/A	134 mV/decade	＜4.1%	[6]
Fe_3C/C-700	N/A	N/A	3.9-4.1	59	< 8%	[7]
Fe–N–C/VA-CNTs	0.79 V	-6 mA cm^{-2}	3.92-3.98	N/A	1%-5%	[16]
LDH@ZIF-67-800	0.675 V	-5.1 mA cm^{-2}	3.85-3.96	N/A	＜10%	[12]
Co-C@Co_9S_8	N/A	N/A	3.9	N/A	N/A	[13]
NCNTF	N/A	N/A	~3.88	N/A	N/A	[14]
Co,N-CNF	0.647	N/A	N/A	N/A	N/A	[17]

Table S5. A comparison of the sensing properties of Co@NCNT with other published Cobalt-based glucose sensors.

Electrode	Linear range (mM)	Sensitivity ($mA \cdot mM^{-1} \cdot cm^{-2}$)	Detect limit (μM)	Response time (s)	Reference
Co@NCNT	0.005-0.395	0.732	0.33	< 3	This work
Co/NG	0.0016-0.47	4.7	0.68	N/A	[7]
Co_3O_4/3DGF	Up to 0.08	3.39	0.025	N/A	[17]
Co_3O_4/PbO_2	0.005-1.2	0.4603	0.31	N/A	[18]
Co_3O_4-rGO/GCE	0.0005-1.277	1.366	0.18	N/A	[19]
S/NPG/Co3O4	Up to 70	12.5	0.005	< 1	[20]
Co_3O_4 Nanofiber	Up to 2.04	0.036	0.97	< 7	[21]
Co_3O_4 Microspheres	0.005-12	1.440	0.08	2	[22]
Co_3O_4 Nanoparticles	0.008-0.5	0.52	0.13	N/A	[23]
Co_3O_4 Nanoflowers	0.1-5.0	1.618	0.1	N/A	[24]
Co_3O_4-HND	Up to 2.06	0.7080	0.06	< 2	[25]
GF/Co_3O_4-NPs/GOD	0.5-16.5	13.52	N/A	N/A	[26]
CoO_x/OPyox	0.0002-0.24	1.024	0.05	N/A	[27]
CoO NRs	0.2-3.5	0.5718	0.058	20-40	[28]
CoO/rGO	0.0008-8.61	0.6697	0.46	3	[29]

Part IV: References

[1] Y.Z. Chen, C. Wang, Z.Y. Wu, Y. Xiong, Q. Xu, S.H. Yu, H.L. Jiang, *Adv. Mater.*, 2015, 27, 5010-5016.

[2] B. You, N. Jiang, M. Sheng, W.S. Drisdell, J. Yano, Y. Sun, *ACS Catal.*, 2015, 5, 7068-7076.

[3] W. Yang, X. Liu, X. Yue, J. Jia, S. Guo, *J. Am. Chem. Soc.*, 2015, 137, 1436-1439.

[4] Y. Hu, J.O. Jensen, W. Zhang, L.N. Cleemann, W. Xing, N.J. Bjerrum, Q. Li, *Angew. Chem. Int. ed.*, 2014, 53, 3675-3679.

[5] S. Dou, L. Tao, J. Huo, S. Wang and L. Dai, *Energy Environ. Sci.*, 2016, 9, 1320-1326.

[6] W. Xia, R. Zou, L. An, D. Xia, S. Guo, *Energy Environ. Sci.*, 2015, 8, 568-576.

[7] S. Ci, Z. Wen, S. Mao, Y. Hou, S. Cui, Z. He, J. Chen, *Chem. Commun.*, 2015, 51, 9354-9357.

[8] Y. Hou, Z. Wen, S. Cui, S. Ci, S. Mao, J. Chen, *Adv. Funct. Mater.,* 2015, 25, 872-882.

[9] Z. Li, M. Shao, L. Zhou, R. Zhang, C. Zhang, M. Wei, D.G. Evans, X. Duan, *Adv. Mater.*, 28, 2337-2344.

[10] H. Hu, L. Han, M. Yu, Z. Wang, X.W.D. Lou, *Energy Environ. Sci.,* 2016, 9, 107-111.

[11] B.Y. Xia, Y. Yan, N. Li, H.B. Wu, X.W.D. Lou, X. Wang, *Nat. Energy,* 2016,1 15006-15013.

[12] P. Zhang, F. Sun, Z. Xiang, Z. Shen, J. Yun, D. Cao, *Energy Environ. Sci.,* 2014, 7, 442-450.

[13] W. Zhang, Z.-Y. Wu, H.-L. Jiang, S.-H. Yu, *J. Am. Chem. Soc.*, 2014, 136, 14385-14388.

[14] H.x. Zhong, J. Wang, Y.w. Zhang, W.l. Xu, W. Xing, D. Xu, Y.f. Zhang, X.b. Zhang, *Angew. Chem. Int. ed.*, 2014, 53, 14235-14239.

[15] L. Shang, H. Yu, X. Huang, T. Bian, R. Shi, Y. Zhao, G.I. Waterhouse, L.Z. Wu, C.H. Tung, T. Zhang, *Adv. Mater.*, 2015.

[16] S. Yasuda, A. Furuya, Y. Uchibori, J. Kim, K. Murakoshi, *Adv. Funct. Mater.*, 2015.

[17] X.-C. Dong, H. Xu, X.-W. Wang, Y.-X. Huang, M.B. Chan-Park, H. Zhang, L.-H. Wang, W. Huang, P. Chen, *ACS Nano*, 2012, 6, 3206-3213.
[18] T. Chen, X. Li, C. Qiu, W. Zhu, H. Ma, S. Chen, O. Meng, *Biosen. Bioelectron.,* 2014, 53, 200-206.
[19] Y. Zheng, P. Li, H. Li, S. Chen, *Int. J. Electrochem. Sci.,* 2014, 9, 7369-7381.
[20] X.-Y. Lang, H.-Y. Fu, C. Hou, G.-F. Han, P. Yang, Y.-B. Liu, Q. Jiang, *Nature commun.*, 2013, 4, 2169.
[21] Y. Ding, Y. Wang, L. Su, M. Bellagamba, H. Zhang, Y. Lei, *Biosen. Bioelectron.,* 2010, 26, 542-548.
[22] C. Guo, X. Zhang, H. Huo, C. Xu, X. Han, *Analyst*, 2013, 138, 6727-6731.
[23] C. Hou, Q. Xu, L. Yin, X. Hu, *Analyst*, 2012, 137, 5803-5808.
[24] Q. Balouch, Z.H. Ibupoto, G.Q. Khaskheli, R.A. Soomro, M.K. Samoon, V.K. Deewani, *J. Electron. Mater.*, 2015, 44, 3724-3732.
[25] E. Zhang, Y. Xie, S. Ci, J. Jia, Z. Wen, *Biosen. Bioelectron.* 2016, 81, 46-53.
[26] C. Karuppiah, S. Palanisamy, S.-M. Chen, V. Veeramani, P. Periakaruppan, *Sensors and Actuators B: Chemical*, 2014, 196, 450-456.
[27] H. Yu, J. Jin, X. Jian, Y. Wang, G.c. Qi, *Electroanal.*, 2013, 25, 1665-1674.
[28] C.-W. Kung, C.-Y. Lin, Y.-H. Lai, R. Vittal, K.-C. Ho, *Biosen. Bioelectron.*, 2011, 27, 125-131.
[29] S. Ci, S. Mao, T. Huang, Z. Wen, D.A. Steeber, J. Chen, *Electroanal.*, 2014, 26, 1326-1334.